Scientia Iranica B (2014) 21(4), 1355–1366

SCIENTIA IRANICA

Sharif University of Technology
Scientia Iranica
Transactions B: Mechanical Engineering
www.scientiairanica.com

MHD stagnation slip flow over an unsteady stretching surface in porous medium

Z. Abbas[a,*], N. Muhammad[b] and G. Mustafa[a]

a. *Department of Mathematics, the Islamia University of Bahawalpur, Bahawalpur 63100, Pakistan*
b. *Department of Mathematics, COMSATS Institute of Information Technology, Attock Campus, Pakistan*

Received 26 April 2012; received in revised form 18 September 2013; accepted 14 December 2013

KEYWORDS
Viscous fluid;
Stagnation-point flow;
Stretching sheet;
Porous medium;
Slip condition.

Abstract. An analysis has been carried out to study the heat transfer analysis and MHD stagnation-point flow of a viscous fluid over an unsteady stretching sheet in a porous medium with slip condition. For the present problem, the governing equations are transformed into a system of non-linear ordinary differential equations by means of similarity transformations. This system is solved both analytically by an analytic technique, namely the Homotopy Analysis Method (HAM), and numerically using a shooting method with Runge-Kutta algorithm. The influences of the involved parameters on the flow and temperature fields are graphically illustrated and analyzed. The results obtained by means of both methods are compared and found in excellent agreement.

1. Introduction

The study of boundary layer flow and heat transfer characteristics due to a continuously stretching heated surface placed in a porous medium has considerable attention in many engineering and industrial applications. The interest is due to many practical applications in thermal engineering and geophysics which can be formulated or approximated as transport phenomena in porous medium. These type of flows appear in a wide range of industrial disciplines, as well as in many natural circumstances such as geothermal extraction, storage of radioactive nuclear waste material, ground water flows, oil recovery processes, food processing, industrial and agricultural water distribution, thermal insulation engineering, packed-bed reactors, casting and welding of manufacturing processes, soil pollution and the dispersion of chemical contaminants in various processes in the chemical industry. Similar situations exist during the manufacture of plastic and rubber sheets where it is often necessary to blow a gaseous medium through a not-yet solidified material, and where the stretching forces may be varying with time (see Pal [1]). The work on this problem has been initiated by Sakiadis [2,3], who discussed the boundary layer flow generated by a continuous solid surface moving with a constant velocity. Crane [4] studied the flow of a viscous fluid over a linearly stretching surface and obtained an exact analytic solution. Additionally many authors [5-10] investigated the Crane's problem for various aspects of the flow and/or heat transfer analysis.

On the other side, in many practical problems, the motion of the continuous stretching surface may start impulsively from rest and the transient or unsteady aspects become more interesting. However, to the best of our knowledge Wang [11] initially discussed the flow of a liquid film over an unsteady stretching sheet. Recently, Elbashbeshy and Bazid [12] presented the similarity solution of boundary layer flow and heat transfer due to an unsteady stretching sheet. Sharidan et al. [13] investigated the unsteady boundary layers over a stretching sheet for special distribution of

*. *Corresponding author. Tel.: +92 62 9255480*
E-mail address: za_qau@yahoo.com (Z. Abbas)

stretching velocity and surface temperature or surface heat flux. Tsai et al. [14] discussed the non-uniform heat source/sink effect on the flow and heat transfer over an unsteady stretching sheet through a quiescent fluid medium extending to infinity. The problem for unsteady stretching surface condition and heat transfer has been studied by several authors such as Abd El-Aziz [15], Mukhopadhyay [16], Ishak et al. [17], Hayat et al. [18] and Ziabakhsh et al. [19]. Very recently, Mukhopadhyay [20] discussed the effects of slip and mixed connective flow past a porous unsteady stretching surface numerically. Elbashbeshy and Emam [21] discussed the effects of the thermal radiation and heat transfer over an unsteady stretching surface embedded in a porous medium in the presence of heat source or sink. Sharma [22] studied the effects of viscous dissipation and heat source on unsteady boundary layer flow and heat transfer past a stretching sheet in a porous medium using the element free Galerkin method. Ibrahim and Shanker [23] presented the numerical study of unsteady MHD boundary layer flow and heat transfer due to a stretching sheet in the presence of heat source/sink. Khan et al. [24] presented a mathematical model for the unsteady stagnation-point flow of a linear viscoelastic fluid bounded by a stretching/shrinking sheet. Recently, Reddy and Reddy [25] discussed mass transfer and MHD effects on an unsteady porous stretching sheet in a porous medium with variable heat flux in the presence of heat source.

Having in mind all the above studies, the aim of the present paper is to study the combined effects of MHD stagnation-point flow and heat transfer due to an unsteady stretching sheet embedded in a porous medium with velocity/thermal slip condition. The conservation equations of mass, momentum and energy are converted into a non-linear boundary value problem by means of suitable stream function. The resultant non-linear equations along with the boundary conditions are then solved numerically using shooting method with Runge-Kutta integration scheme and analytically using a powerful technique the homotopy analysis method [26-37]. Comparisons of the present results with previously published works in the literature are given and found in excellent agreement.

2. Flow equations

We consider an unsteady, two-dimensional MHD stagnation point flow of a viscous fluid in a porous medium over an unsteady stretching sheet in the region $y > 0$ as shown in Figure 1. The x axis is taken along the surface, while the y axis is perpendicular to the surface. At time $t = 0$, the surface is stretched with the velocity $U_\omega(x,t)$ along the x axis, keeping the origin is fixed. It is also assumed that the fluid is electrically conducting

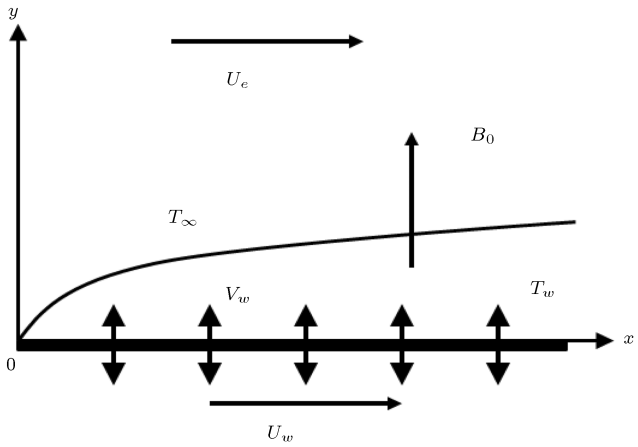

Figure 1. Flow geometry and coordinate system.

and the magnetic field B_0 is applied in the y direction. The induced magnetic field is neglected due to a small magnetic Reynolds number assumption, where no external electric field is applied. The velocity of the flow external to the boundary layer is $U_e(x,t)$ and the temperature at the surface is $T_\omega(x,t)$, where $T_\omega > T_\infty$, with T_∞ being the temperature of the ambient fluid. Under these assumptions along with the boundary layer approximations, the governing equations for the flow and energy are given as:

$$\frac{\partial u}{\partial x} + \frac{\partial v}{\partial y} = 0, \tag{1}$$

$$\frac{\partial u}{\partial t} + u\frac{\partial u}{\partial x} + v\frac{\partial u}{\partial y} = \frac{\partial U_e}{\partial t} + U_e\frac{\partial U_e}{\partial x} + \nu\frac{\partial^2 u}{\partial y^2} + \frac{\sigma B_0^2}{\rho}(U_e - u) + \frac{\nu\phi}{k(t)}(U_e - u), \tag{2}$$

$$\frac{\partial T}{\partial t} + u\frac{\partial T}{\partial x} + v\frac{\partial T}{\partial y} = \alpha\frac{\partial^2 T}{\partial y^2}, \tag{3}$$

where u and v are the velocity components in the x and y directions, respectively, ν is the kinematic viscosity, ρ is the fluid density, σ is the electrical conductivity of the fluid, ϕ is porosity of the medium, α is the thermal diffusivity, t is the time, T is the temperature of the fluid, and $k(t)$ is the permeability of the porous medium. Here we assume $k(t)$ is of the form:

$$k(t) = k_1(1 - \delta t), \tag{4}$$

where k_1 is the initial permeability.

The relevant boundary conditions for the present problem are:

$$u = U_\omega(x,t) + N_1\nu\frac{\partial u}{\partial y}, \quad v = 0,$$

$$T = T_\omega(x,t) + D_1\frac{\partial T}{\partial y} \quad \text{at} \quad y = 0, \tag{5}$$

$$u \to U_e(x,t), \quad T \to T_\infty \quad \text{as} \quad y \to \infty. \tag{6}$$

Here:

$$U_\omega = \frac{bx}{(1-\delta t)}, \qquad U_e = \frac{dx}{(1-\delta t)},$$

$$T_\omega(x,t) = T_\infty + \frac{cx}{\nu(1-\delta t)},$$

where $b \geq 0$, $d \geq 0$, $c \geq 0$ and $\delta \geq 0$ are constants (with $\delta t < 1$) and have dimensions $(\text{time})^{-1}$, $N_1 = N\sqrt{1-\delta t}$ is the velocity slip parameter, and $D_1 = D\sqrt{1-\delta t}$ is the thermal slip parameter, both are changed with time, and N and D arethe initial values of velocity and thermal slip parameters, having dimension $(\text{velocity})^{-1}$ and length, respectively. The no-slip condition can be obtained for $N = 0$ and $D = 0$, respectively.

We define the following similarity transformations:

$$\eta = \sqrt{\frac{b}{\nu}}(1-\delta t)^{-\frac{1}{2}} y, \quad \psi = \sqrt{b\nu}x(1-\delta t)^{-\frac{1}{2}} f(\eta), \quad (7)$$

$$\theta(\eta) = \frac{T - T_\infty}{T_\omega - T_\infty},$$

$$T_\omega = T_\infty + T_{\text{ref}}\left(\frac{bx^2(1-\delta t)^{\frac{-3}{2}}}{2\nu}\right), \quad (8)$$

where T_{ref} is taken as a constant reference temperature and the stream function $\psi(x,y)$ is defined by $u = \partial\psi/\partial y$ and $v = -\partial\psi/\partial x$, such that the continuity equation (Eq. (1)) is automatically satisfied.

Using Eqs.(7) and (8), Eqs. (2) and (3) become:

$$f''' - f'^2 + ff'' - A\left(f' + \frac{1}{2}\eta f''\right) + M^2(\varepsilon - f') + \lambda(\varepsilon - f') + A\varepsilon + \varepsilon^2 = 0, \quad (9)$$

$$\frac{1}{\text{Pr}}\theta'' - 2f'\theta + f\theta' - \frac{A}{2}(3\theta + \eta\theta') = 0, \quad (10)$$

and the corresponding boundary conditions are:

$$f = 0, \quad f' = 1 + \beta f'', \quad \theta = 1 + \gamma\theta' \quad \text{at} \quad \eta = 0,$$

$$f' \to \varepsilon, \quad \theta \to 0 \quad \text{as} \quad \eta \to \infty, \quad (11)$$

where $A = \delta/b$ is the unsteadiness parameter, $\text{Pr} = \nu/\alpha$ is the Prandtl number, $\varepsilon = d/b$ is the ratio of the external flow rate to the stretching rate, $M^2 = \sigma B_0^2(1-\delta t)/\rho b$ is the local magnetic parameter, $\lambda = \nu\phi/kb$ is the porosity parameter, $\beta = N\sqrt{b\nu}$ is the velocity slip parameter, $\gamma = D\sqrt{b/\nu}$ is the thermal slip parameter and the primes indicate the differentiation with respect to η. It is worth mentioning that we could recover the no-slip condition by taking $\beta = 0$ and $\gamma = 0$.

It should be mentioned here that in the paper of Elbashbeshy and Bazid [12] the sign of the term $2f'\theta$ is positive in their energy equation due to the incorrect definition of $\Delta T = T_\omega - T_\infty$ and hence an exact comparison is not possible. According to them $\Delta T = T_\omega - T_\infty = \frac{b}{2\nu x^2}(1-\delta t)^{\frac{-3}{2}}$ but the correct value is $\frac{bx^2}{2\nu}(1-\delta t)^{\frac{-3}{2}}$. Due to this error, some physically unrealistic phenomena in the velocity and temperature fields are encountered for specific values of the unsteadiness parameter. Abd El-Aziz [15] also mentioned this error in his paper. In the present work when M, λ, ε, β and γ are taken to be zero then Eqs. (9) and (10) with the boundary conditions (Eq. (11)) reduce to those of Abd El-Aziz [15].

The skin-friction coefficient, C_f, and the local Nusselt number, Nu_x, are given by:

$$C_f = \frac{\tau_\omega}{\rho U_\omega^2}, \qquad Nu_x = \frac{xq_\omega}{k_m(T_\omega - T_\infty)}, \quad (12)$$

where k_m is thermal conductivity, τ_ω is the shear stress at the wall and q_ω is the heat flux at wall, which are defined as:

$$\tau_\omega = \mu\left(\frac{\partial u}{\partial y}\right)_{y=0}, \quad \text{and} \quad q_\omega = -k_m\left(\frac{\partial T}{\partial y}\right)_{y=0}. \quad (13)$$

With the help of Eqs. (7), (8) and (13), Eq. (12) yields:

$$\frac{Nu_x}{\sqrt{\text{Re}_x}} = -\theta'(0), \quad \text{or} \quad \sqrt{\text{Re}_x}C_f = f''(0), \quad (14)$$

where $Re_x = xU_\omega/\nu$ is the local Reynolds number.

3. Solution of the problem

3.1. Numerical solution

To find the numerical solution, we use the most effective shooting method with fourth order Runge-Kutta integration scheme (see Na [38]) to solve the boundary value problem. The non-linear equations (Eqs. (9) and (10)) subject to boundary conditions (Eq. (11)) are transformed into a system of five first order differential equations as:

$$\frac{df_0}{d\eta} = f_1, \quad (15)$$

$$\frac{df_1}{d\eta} = f_2, \quad (16)$$

$$\frac{df_2}{d\eta} = -ff_2 + (f_1)^2 + Af_1 + \frac{1}{2}A\eta f_2 - M^2(\varepsilon - f_1) - \lambda(\varepsilon - f_1) - A\varepsilon - \varepsilon^2, \quad (17)$$

$$\frac{d\theta_0}{d\eta} = \theta_1, \tag{18}$$

$$\frac{d\theta_1}{d\eta} = \Pr\left(2f_1\theta - f\theta_1 + \frac{3}{2}A\theta + \frac{1}{2}A\eta\theta_1\right), \tag{19}$$

and the boundary conditions are:

$$f(0) = 0, \qquad f_1(0) = 1 + \beta f_2(0), \qquad f_1(\infty) = \varepsilon,$$

$$\theta(0) = 1 + \gamma\theta_1(0), \qquad \theta(\infty) = 0. \tag{20}$$

Here, $f_0 = f(\eta)$ and $\theta_0 = \theta(\eta)$. A boundary value problem is first converted into an initial value problem by appropriately guessing the missing conditions, $f_2(0)$ and $\theta_1(0)$. The resultant initial value problem is solved by shooting method for a set of parameters appearing in the governing equations with a known values of $f_2(0)$ and $\theta_1(0)$.

3.2. Homotopy analysis solution

For the series solutions of Eqs. (9) and (10), using homotopy analysis method (HAM), it is straight forward that the velocity and the temperature fields $f(\eta)$ and $\theta(\eta)$ can be expressed by the set of base functions:

$$\left\{\eta^k \exp(-n\eta) \middle| k \geq 0, n \geq 0\right\}, \tag{21}$$

in the form:

$$f(\eta) = a^0_{0,0} + \sum_{n=0}^{\infty}\sum_{k=0}^{\infty} a^k_{m,n}\eta^k \exp(-n\eta), \tag{22}$$

$$\theta(\eta) = \sum_{n=0}^{\infty}\sum_{k=0}^{\infty} b^k_{m,n}\eta^k \exp(-n\eta), \tag{23}$$

where $a^k_{m,n}$ and $b^k_{m,n}$ are the coefficients. By rule of solution expressions of $f(\eta)$ and $\theta(\eta)$, with the help of boundary conditions (Eq. (11)) one can choose $f_0(\eta)$ and $\theta_0(\eta)$:

$$f_0(\eta) = \varepsilon\eta + \frac{(1-\varepsilon)(1-e^{-\eta})}{1+\beta}, \tag{24}$$

$$\theta_0(\eta) = \frac{e^{-\eta}}{1+\gamma}, \tag{25}$$

as the initial guess approximations of $f(\eta)$ and $\theta(\eta)$ and the auxiliary linear operators:

$$\mathcal{L}_f(f) = \frac{d^3f}{d\eta^3} - \frac{df}{d\eta}, \tag{26}$$

$$\mathcal{L}_\theta(f) = \frac{d^2f}{d\eta^2} - f, \tag{27}$$

which have the following properties:

$$\mathcal{L}_f\left[C_1 + C_2\exp(\eta) + C_3\exp(-\eta)\right] = 0, \tag{28}$$

$$\mathcal{L}_\theta\left[C_4\exp(\eta) + C_5\exp(-\eta)\right] = 0, \tag{29}$$

where C_i, $(i = 1-5)$ are arbitrary constants. If $\hbar_f$ and $\hbar_\theta$ denote the non-zero auxiliary parameters then the zeroth-order deformation problems are constructed as:

$$(1-q)\,\mathcal{L}_f\left[\widehat{f}(\eta;q) - f_0(\eta)\right] = q\hbar_f\mathcal{N}_f\left[\widehat{f}(\eta;q)\right], \tag{30}$$

$$(1-q)\,\mathcal{L}_\theta\left[\widehat{\theta}(\eta;q) - \theta_0(\eta)\right] = q\hbar_\theta\mathcal{N}_\theta\left[\widehat{f}(\eta;q), \widehat{\theta}(\eta;q)\right], \tag{31}$$

$$\widehat{f}(0;q) = 0,$$

$$\frac{d\widehat{f}(0,q)}{d\eta} = 1 + \beta\frac{d^2\widehat{f}(0,q)}{d\eta^2},$$

$$\frac{d\widehat{f}(\infty,q)}{d\eta} = \varepsilon, \tag{32}$$

$$\widehat{\theta}(0,q) = 1 + \gamma\frac{d\widehat{\theta}(0,q)}{d\eta},$$

$$\widehat{\theta}(\infty,q) = 0, \tag{33}$$

where $q \in [0,1]$ is an embedding parameter and the nonlinear operators $\mathcal{N}_f$ and $\mathcal{N}_\theta$ are:

$$\begin{aligned}\mathcal{N}_f\left[\widehat{f}\left(\eta;q\right)\right] =& \frac{\partial^3\widehat{f}\left(\eta,q\right)}{\partial\eta^3} - \left(\frac{\partial\widehat{f}\left(\eta,q\right)}{\partial\eta}\right)^2 \\ &+ \widehat{f}\left(\eta,q\right)\frac{\partial^2\widehat{f}\left(\eta,q\right)}{\partial\eta^2} - A\frac{\partial\widehat{f}\left(\eta,q\right)}{\partial\eta} \\ &- \frac{1}{2}A\eta\frac{\partial^2\widehat{f}\left(\eta,q\right)}{\partial\eta^2} \\ &+ M^2\left(\varepsilon - \frac{\partial\widehat{f}\left(\eta,q\right)}{\partial\eta}\right) \\ &+ \lambda\left(\varepsilon - \frac{\partial\widehat{f}\left(\eta,q\right)}{\partial\eta}\right) + A\varepsilon + \varepsilon^2,\end{aligned} \tag{34}$$

$$\mathcal{N}_\theta\left[\widehat{f}\left(\eta;q\right),\widehat{\theta}\left(\eta;q\right)\right]=\overset{-1}{\Pr}\theta''-2\frac{\partial\widehat{f}\left(\eta,q\right)}{\partial\eta}\theta\left(\eta,q\right)+f\left(\eta,q\right)\frac{\partial\widehat{\theta}\left(\eta,q\right)}{\partial\eta}-\frac{3}{2}A\theta\left(\eta,q\right)-\frac{1}{2}A\eta\frac{\partial\widehat{\theta}\left(\eta,q\right)}{\partial\eta}. \quad (35)$$

For $q=0$ and $q=1$, the above zeroth-order deformation equations (Eqs. (30) and (31)) have the solutions:

$$\widehat{f}\left(\eta;0\right)=f_0\left(\eta\right),\qquad \widehat{f}\left(\eta;1\right)=f\left(\eta\right), \quad (36)$$

$$\widehat{\theta}\left(\eta;0\right)=\theta_0\left(\eta\right),\qquad \widehat{\theta}\left(\eta;1\right)=\theta\left(\eta\right). \quad (37)$$

Expanding $\widehat{f}\left(\eta;q\right)$ and $\widehat{\theta}\left(\eta;q\right)$ in Taylor's series with respect to q, we have:

$$\widehat{f}\left(\eta;q\right)=f_0\left(\eta\right)+\sum_{m=1}^{\infty}f_m\left(\eta\right)q^m, \quad (38)$$

$$\widehat{\theta}\left(\eta;q\right)=\theta_0\left(\eta\right)+\sum_{m=1}^{\infty}\theta_m\left(\eta\right)q^m, \quad (39)$$

where:

$$f_m\left(\eta\right)=\left.\frac{1}{m!}\frac{\partial^m\widehat{f}\left(\eta;q\right)}{\partial q^m}\right|_{q=0},$$

$$\theta_m\left(\eta\right)=\left.\frac{1}{m!}\frac{\partial^m\widehat{\theta}\left(\eta;q\right)}{\partial q^m}\right|_{q=0}. \quad (40)$$

Note that the zeroth-order deformation equations (Eqs. (30) and (31)) contain two auxiliary parameters $\hbar_f$ and $\hbar_\theta$. The convergence of the series (30) and (31) depends on these parameters. Assuming that $\hbar_f$ and $\hbar_\theta$ are selected such that the above series are convergent at $q=1$, then using Eqs. (36) and (37), the series solutions are:

$$f\left(\eta\right)=f_0\left(\eta\right)+\sum_{m=1}^{\infty}f_m\left(\eta\right), \quad (41)$$

$$\theta\left(\eta\right)=\theta_0\left(\eta\right)+\sum_{m=1}^{\infty}\theta_m\left(\eta\right). \quad (42)$$

Differentiate the zeroth-order deformation equations (Eqs. (30) and (31)) m times with respect to q, then setting $q=0$, and finally dividing them by $m!$, we obtain the mth-order deformations equations as:

$$\mathcal{L}_f\left[f_m\left(\eta\right)-\chi_m f_{m-1}\left(\eta\right)\right]=\hbar_f\mathcal{R}_m^f\left(\eta\right), \quad (43)$$

$$\mathcal{L}_\theta\left[\theta_m\left(\eta\right)-\chi_m\theta_{m-1}\left(\eta\right)\right]=\hbar_\theta\mathcal{R}_m^\theta\left(\eta\right), \quad (44)$$

$$f_m\left(0\right)=0,\quad f'_m(0)=\beta f''_m\left(0\right),\quad f_m\left(\infty\right)=0, \quad (45)$$

$$\theta_m\left(0\right)=\gamma\theta'_m\left(0\right),\ \theta_m\left(\infty\right)=0, \quad (46)$$

where:

$$\mathcal{R}_m^f\left(\eta\right)=f'''_{m-1}-A\left(f'_{m-1}+\frac{1}{2}\eta f''_{m-1}\right)-M^2f'_{m-1}-\lambda f'_{m-1}+\sum_{k=0}^{m-1}\left[f_{m-1-k}f''_k-f'_{m-1-k}f'_k\right]+(1-\chi_m)(M^2\varepsilon+\lambda\varepsilon+A\varepsilon+\varepsilon^2), \quad (47)$$

$$\mathcal{R}_m^\theta\left(\eta\right)=\overset{-1}{\Pr}\theta''_{m-1}-\frac{3}{2}A\theta_{m-1}-A\frac{\eta}{2}\theta'_{m-1}+\sum_{k=0}^{m-1}\left[f_{m-1-k}\theta'_k-2f'_{m-1-k}\theta_k\right], \quad (48)$$

$$\chi_m=\begin{cases}0, & m\leq 1,\\ 1, & m>1.\end{cases} \quad (49)$$

If we suppose $f_m^\star\left(\eta\right)$ and $\theta_m^\star\left(\eta\right)$ as the special solutions of Eqs. (43) and (44), then from Eqs. (43) and (44), the general solutions are given by:

$$f_m\left(\eta\right)=f_m^\star\left(\eta\right)+C_1+C_2\exp\left(\eta\right)+C_3\exp\left(-\eta\right), \quad (50)$$

$$\theta_m\left(\eta\right)=\theta_m^\star\left(\eta\right)+C_4\exp\left(\eta\right)+C_5\exp\left(-\eta\right), \quad (51)$$

where the integral constants C_i, $(i=1-5)$ are determined from the boundary conditions (Eqs. (45) and (46)) as:

$$C_2=C_4=0,$$

$$C_3=\frac{\left.\frac{\partial f_m^\star\left(\eta\right)}{\partial\eta}\right|_{\eta=0}-\beta\left.\frac{\partial f_m^{2\star}\left(\eta\right)}{\partial\eta^2}\right|_{\eta=0}}{1+\beta},$$

$$C_1=-C_3-f_m^\star\left(0\right),$$

$$C_5=-\frac{\theta_m^\star\left(\eta\right)|_{\eta=0}-\gamma\left.\frac{\partial\theta_m^\star\left(\eta\right)}{\partial\eta}\right|_{\eta=0}}{1+\gamma}. \quad (52)$$

In this way, it is easy to solve the linear non-homogeneous Eqs. (43) and (44) by using Mathematica one after the other in the order $m=1,2,3$.....

3.3. Convergence of the HAM solution

As proved by Liao [26], as long as a solution series given by the homotopy analysis method converges, it must be one of the solutions. Therefore, it is important to ensure that the solutions series are convergent. The series solutions (41) and (42) contain the non-zero auxiliary parameters $\hbar_f$ and $\hbar_\theta$, which can be chosen properly by plotting the so-called $\hbar$-curves to ensure the convergence of the solutions series and rate of approximation of the HAM solution. To see the range for admissible values of $\hbar_f$ and $\hbar_\theta$, $\hbar$-curves of $f''(0)$ and $\theta'(0)$ are shown in Figure 2, for 20th order of approximation when $A = 0.2$, $M = 0.5$, $\lambda = 0.2$, $\Pr = 0.5$, $\varepsilon = 0.2$ and $\beta = \gamma = 0.2$. From this figure it can be seen that $\hbar$-curves have a parallel linessegment that correspond to the regions $-1.1 \leq \hbar_f \leq -0.2$ and $-1.15 \leq \hbar_\theta \leq -0.2$, respectively. Table 1 is made to show the convergence and comparison of HAM solution for various order of approximations with numerical results when $A = 0.2$, $M = 0.5$, $\lambda = 0.2$, $\Pr = 0.5$, $\varepsilon = 0.2$ and $\beta = \gamma = 0.2$.

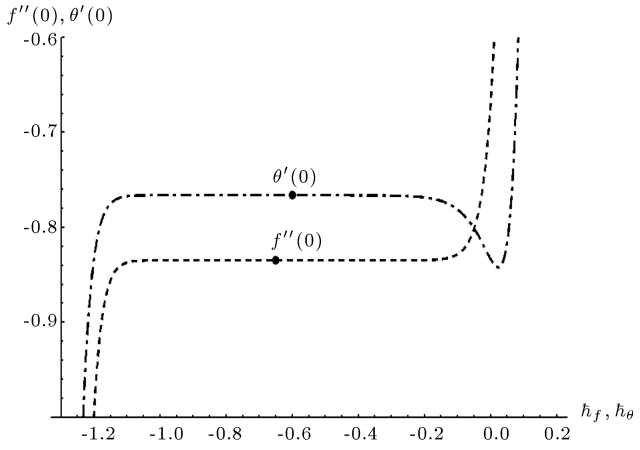

Figure 2. The h-curves of $f''(0)$ and $\theta'(0)$ at the 20th order of approximation; filled circles are the numerical values with $A = 0.2$, $M = 0.5$, $\lambda = 0.2$, $\Pr = 0.5$, $\varepsilon = 0.2$, $\gamma = 0.2$ and $\beta = 0.2$.

Table 1. Convergence and comparison of HAM solution for different order of approximation with numerical results when $A = 0.2$, $M = 0.5$, $\lambda = 0.2$, $\Pr = 0.5$, $\varepsilon = 0.2$, $\beta = 0.2$ and $\gamma = 0.2$.

Order of approximations	$-f''(0)$	$-\theta'(0)$
1	0.815741	0.816454
5	0.834424	0.769523
9	0.834491	0.766372
15	0.834491	0.766005
20	0.834491	0.765987
23	0.834491	0.765985
25	0.834491	0.765985
30	0.834491	0.765985
Numerical results	0.834519	0.765986

3.4. Results and discussion

The system of Eqs. (9) and (10) with boundary conditions (11) has been solved both analytically using Homotopy Analysis Method (HAM) and numerically using shooting method [38] with Runge-Kutta algorithm. Figures 3-12 are plotted in order to analyze the influences of the various involving physical parameters, for example, an unsteadiness parameter A, the magnetic parameter M, the porosity parameter λ, the velocity slip parameter β, the ratio of external flow rate to the stretching rate ε, the Prandtl number $\Pr$ and the thermal slip parameter γ on the velocity $f'(\eta)$ and temperature $\theta(\eta)$ distributions. The numerical values of the skin-friction coefficient $-f''(0)$ and the rate of heat transfer at the wall (the local Nusselt number) $-\theta'(0)$ for various values of parameters are given in Tables 2-5.

Figure 3 shows the effects of an unsteadiness

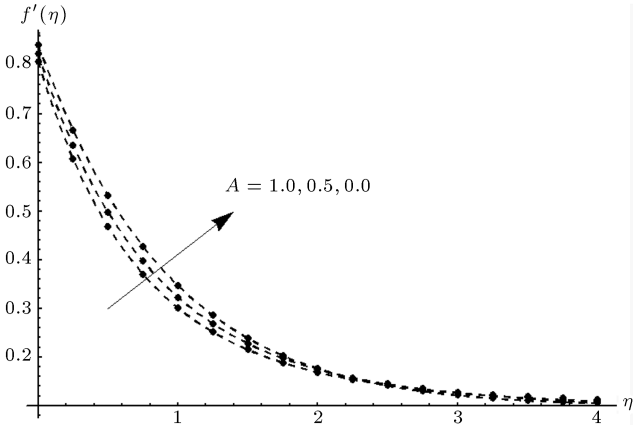

Figure 3. The velocity profile $f'(\eta)$ verses η for various values of unsteadiness parameter A: dashed lines are numerical solution and filled circle are HAM solution at 12th order of approximation with $M = 0.2$, $\lambda = 0.1$, $\varepsilon = 0.1$ and $\beta = 0.2$.

Table 2. A comparison of the values of $-\theta'(0)$ with Refs. [12,14] for several values of A and $\Pr$ with $M = \lambda = \varepsilon = \beta = \gamma = 0$.

Pr	A	Ref. [12]	Ref. [15]	Present results	
				HAM	Numerical
0.1	0.8	0.2707	0.4517	0.4517	0.45357
1		0.6348	1.6728	1.6728	1.6720
10		1.2552	5.70503	5.7059	5.70494
0.1	1.2	0.3576	0.5087	0.5086	0.5030
1		0.9491	1.818	1.818	1.818
10		2.4177	6.12067	6.0612	6.12013
0.1	2.0	0.4991	0.604013	0.60376	0.60478
1		1.4086	2.07841	2.0784	2.07817
10		3.9814	6.88506	6.63421	6.88176

parameter A on the velocity component $f'(\eta)$ when $M = 0.2$, $\lambda = 0.1$, $\varepsilon = 0.1$ and $\beta = 0.2$. Both the velocity and the boundary layer thickness are decreased as an unsteadiness parameter A increases. Figure 4 elucidates the influence of the magnetic parameter M on the velocity $f'(\eta)$ when $A = 0.2$, $\lambda = 0.1$, $\varepsilon = 0.1$ and $\beta = 0.2$. It is noted from this figure that the velocity decreases by increasing the values of magnetic parameter M. This is because for the present problem, the magnetic force acts as a resistance to the flow. The boundary layer thickness is also decreased as M increases. The change in the velocity field $f'(\eta)$ for different values of porosity parameter λ can be seen in Figure 5. It is found that the velocity $f'(\eta)$ is a decreasing function of λ. The boundary layer thickness is decreased for large values of λ. Figure 6 depicts the variations of the velocity slip parameter β on the velocity component $f'(\eta)$ when $\varepsilon = 0.1$. It is observed that the velocity is decreased by increasing the values of the velocity slip parameter β. It is also noted that for $\beta = 0$ (no-slip condition), the values of f' is equal to 1, which shows the standard condition for stretching flow at $\eta = 0$. Figure 7 shows the effects of the ratio of the external flow rate to the

Table 3. Numerical values of skin friction coefficient, $-f''(0)$, and the local Nusselt number, $-\theta'(0)$, for several values of A, M and λ with $\varepsilon = 0.5$, $\gamma = \beta = 0.2$ and Pr = 0.5.

			$-f''(0)$		$-\theta'(0)$	
A	M	λ	HAM	Numerical	HAM	Numerical
0.2	0.5	0.5	0.60449	0.60449	0.83901	0.83901
0.8			0.64108	0.64109	0.95431	0.95425
1.2			0.66376	0.66376	1.0201	1.0201
2.0			0.70545	0.70545	1.1330	1.1330
0.8	0		0.62073	0.62075	0.95657	0.95651
	0.5		0.64108	0.64109	0.95431	0.95425
	1.0		0.69538	0.69548	0.94847	0.94841
	1.5		0.76970	0.76970	0.94099	0.94099
	2.0		0.85193	0.85193	0.93334	0.93334
	0.5	0	0.59900	0.59904	0.95904	0.95900
		0.5	0.64108	0.64109	0.95430	0.95425
		1.0	0.67827	0.67829	0.95028	0.95021
		1.5	0.71165	0.71165	0.94679	0.94679
		2.0	0.74194	0.74195	0.94372	0.94370

Table 5. Numerical values of the local Nusselt number $-\theta'(0)$ for several values of A, Pr and γ with $M = \lambda = \beta = 0.2$ and $\varepsilon = 0.5$.

Pr	γ	$A = 0.8$		$A = 1.2$	
		HAM	Numerical	HAM	Numerical
0.1	0.2	0.46416	0.46410	0.50277	0.50271
0.3		0.76908	0.76901	0.82519	0.82511
0.7		1.1024	1.1021	1.1729	1.1724
1.0		1.2700	1.2700	1.3462	1.3453
1.5		1.4791	1.4761	1.5610	1.5604
2.0		1.6384	1.6315	1.7239	1.7211
3.0		1.8761	1.8704	1.9653	1.9647
5.0		2.1916	2.1901	2.2834	2.2801
0.7	0	1.4143	1.4149	1.5324	1.5329
	0.5	0.82844	0.82854	0.86763	0.86796
	1.0	0.58579	0.58586	0.60512	0.60526
	1.5	0.45309	0.45317	0.46456	0.46461
	2.0	0.36940	0.36983	0.37699	0.37699
	3.0	0.26975	0.26979	0.27378	0.27384
	5.0	0.17522	0.17584	0.17691	0.17613
	10.0	0.09339	0.09339	0.09387	0.09387

Table 4. Numerical values of skin friction coefficient, $-f''(0)$, and the local Nusselt number, $-\theta'(0)$, for several values of ε and β with $M = 0.2$ and $\lambda = 0.2$.

ε	β	$A = 0.8$				$A = 1.2$				$A = 2.0$			
		HAM		Numerical		HAM		Numerical		HAM		Numerical	
		$-f''(0)$	$-\theta'(0)$	$-f''(0)$	$-\theta'(0)$	$-f''(0)$	$-\theta'(0)$	$-f''(0)$	$-\theta'(0)$	$-f''(0)$	$-\theta'(0)$	$-f''(0)$	$-\theta'(0)$
0	0.2	1.0176	0.8710	1.0176	0.8716	1.0865	0.9470	1.0865	0.9473	1.2059	1.0724	1.2059	1.0726
0.5		0.5980	0.9591	0.5981	0.9590	0.6238	1.0240	0.6238	1.0240	0.6707	1.1357	0.6709	1.1357
1.0		0	1.0476	0	1.0472	0	1.1029	0	1.1025	0	1.2013	0	1.2019
1.5		0.7305	1.1300	0.7305	1.1304	0.7479	1.1781	0.7479	1.1780	0.7804	1.2653	0.7805	1.2667
2.0		1.5652	1.2057	1.5652	1.2056	1.5953	1.2483	1.5953	1.2480	1.6515	1.3264	1.6523	1.3269
0.5	0	0.8050	0.9831	0.8051	0.9831	0.8498	1.0467	0.8498	1.0461	0.9345	1.1562	0.9347	1.1561
	0.5	0.4351	0.9386	0.4351	0.9386	0.4494	1.0052	0.4494	1.0050	0.4744	1.1195	0.4745	1.1190
	1	0.3010	0.9206	0.3010	0.9201	0.3081	0.9889	0.3080	0.9889	0.3203	1.1060	0.3203	1.1068
	1.5	0.2307	0.9106	0.2307	0.9106	0.2349	0.9801	0.2347	0.9801	0.2421	1.0989	0.2422	1.0987
	2.0	0.1871	0.9043	0.1872	0.9041	0.1900	0.9746	0.1900	0.9746	0.1947	1.0946	0.1948	1.0949

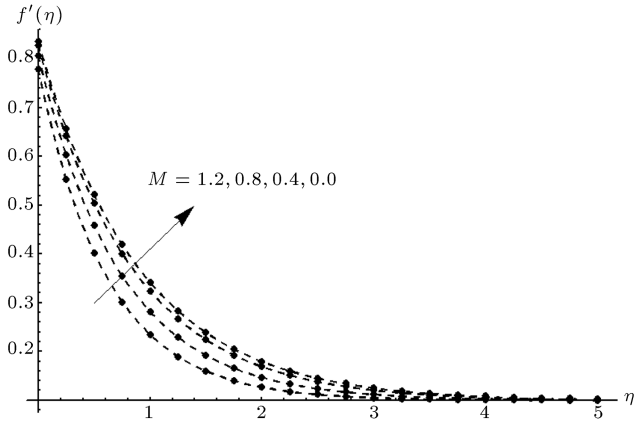

Figure 4. The velocity profile $f'(\eta)$ verses η for various values of magnetic parameter M: dashed lines are numerical solution and filled circle are HAM solution at 12th order of approximation with $A = 0.2$, $\lambda = 0.1$, $\varepsilon = 0.1$ and $\beta = 0.2$.

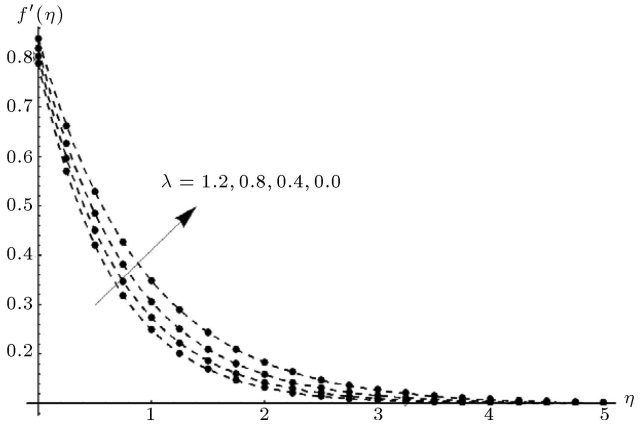

Figure 5. The velocity profile $f'(\eta)$ verses η for various values of porous medium λ: dashed lines are numerical solution and filled circle are HAM solution at 12th order of approximation with $A = 0.2$, $M = 0.2$, $\varepsilon = 0.1$ and $\beta = 0.2$.

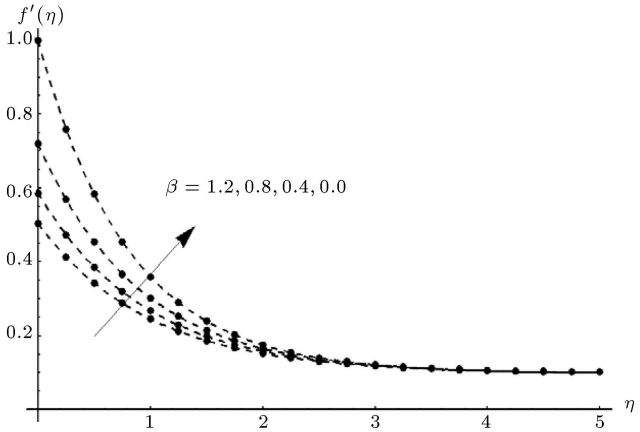

Figure 6. The velocity profile $f'(\eta)$ verses η for various values of slip parameter β: dashed lines are numerical solution and filled circle are HAM solution at 12th order of approximation with $A = 0.2$, $M = \lambda = 0.2$ and $\varepsilon = 0.1$.

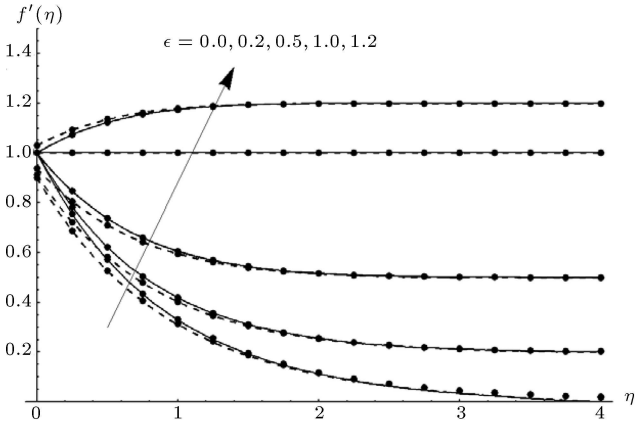

Figure 7. The velocity profile $f'(\eta)$ verses η for various values of stagnation point parameter ε: solid/dashed lines are numerical solution and filled circle are HAM solution at 12th order of approximation with $A = 0.2$, $M = 0.2$ and $\lambda = 0.1$.

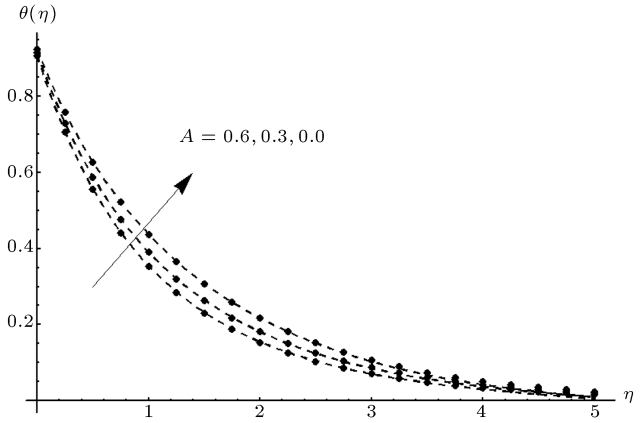

Figure 8. The temperature profile $\theta(\eta)$ verses η for various values of unsteadiness parameter A: dashed lines are numerical solution and filled circle are HAM solution at 12th order of approximation with $M = 0.2$, $\lambda = 0.1$, Pr $= 0.5$, $\varepsilon = \gamma = 0.1$ and $\beta = 0.2$.

stretching rate ε on the velocity field $f'(\eta)$: solid lines for no-slip condition $\beta = 0$ and dashed lines for slip condition $\beta = 0.2$, respectively. It is found that the velocity $f'(\eta)$ is increased for large values of ε for both $\beta = 0$, $\beta = 0.2$ but this change in the velocity in case of velocity slip parameter ($\beta = 0.2$) is smaller for $\varepsilon < 1$ and larger for $\varepsilon > 1$ near the wall when compared with the case of no-slip condition ($\beta = 0$).

Figure 8 gives the influences of an unsteadiness parameter A on the temperature distribution $\theta(\eta)$ when thermal slip parameter $\gamma = 0.1$. Both the temperature profile and the thermal boundary layer thickness are decreased as A increases. Figure 9 shows the change in the temperature $\theta(\eta)$ for the several values of Prandtl number Pr: solid lines for no-thermal slip, $\gamma = 0$, and dashed lines for thermal slip, $\gamma = 0.1$. It is evident from this figure that the

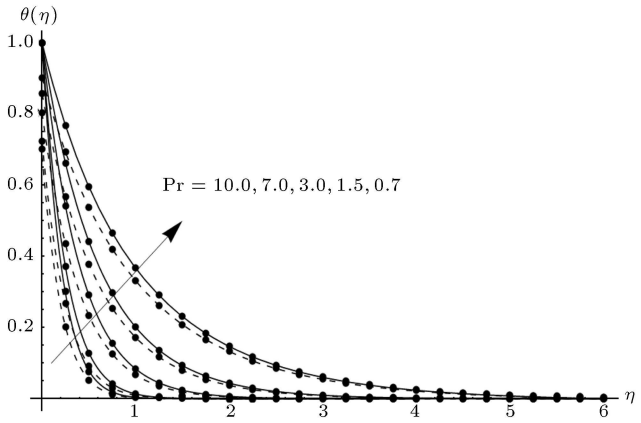

Figure 9. The temperature profile $\theta(\eta)$ verses η for various values of Prandtl number Pr: solid/dashed lines are numerical solution and filled circle are HAM solution at 12th order of approximation with $A = 0.2$, $M = 0.2$, $\lambda = 0.1$, $\varepsilon = 0.1$ and $\beta = 0.2$.

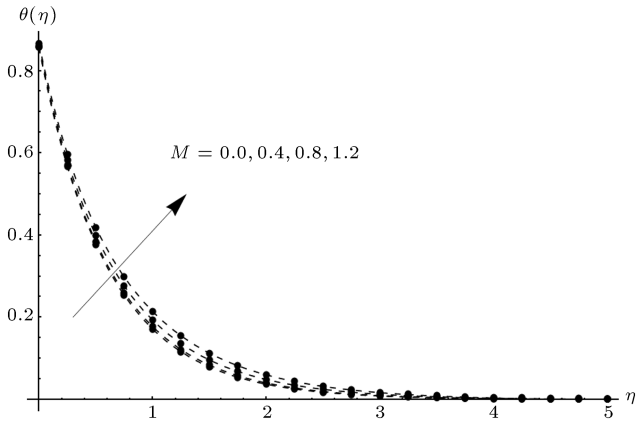

Figure 10. The temperature profile $\theta(\eta)$ verses η for various values of magnetic parameter M: dashed lines are numerical solution and filled circle are HAM solution at 12th order of approximation with $A = 0.2$, $\varepsilon = \lambda = \gamma = 0.1$, Pr = 1.5 and $\beta = 0.2$.

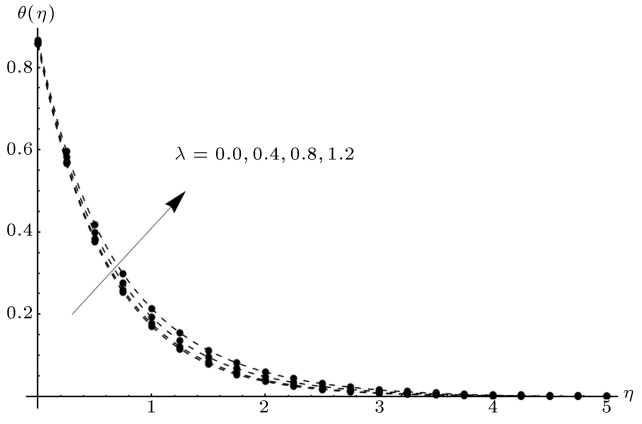

Figure 11. The temperature profile $\theta(\eta)$ verses η for various values of porous medium λ: dashed lines are numerical solution and filled circle are HAM solution at 12th order of approximation with $A = 0.2$, $M = 0.2$, Pr = 1.5, $\varepsilon = \gamma = 0.1$ and $\beta = 0.2$.

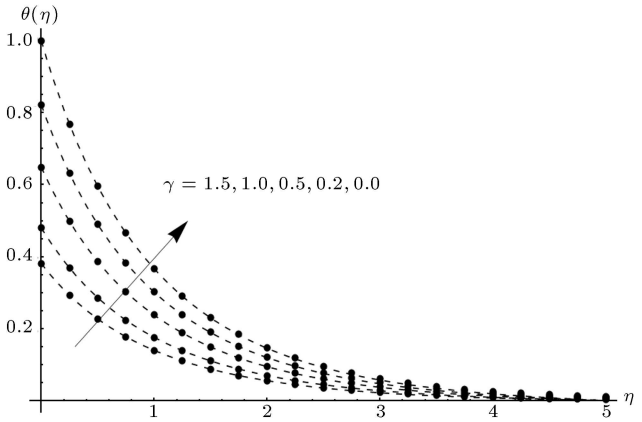

Figure 12. The temperature profile $\theta(\eta)$ verses η for various values of slip parameter γ: dashed lines are numerical solution and filled circle are HAM solution at 12th order of approximation with $A = 0.2$, $M = 0.2$, $\lambda = \varepsilon = 0.1$, Pr = 0.7 and $\beta = 0.2$.

temperature decreases by increasing the values of Pr due to the decreased thermal diffusivity. The thermal boundary layer thickness also decreases for large values of Prandtl number. Figure 10 gives the variations in the temperature distribution $\theta(\eta)$ for various values of a magnetic parameter M. One can see that the temperature is an increasing function of a magnetic parameter M, and the thermal boundary layer thickness also increases as M is increased. Figure 11 presents the effects of a porosity parameter, λ, on the temperature distribution, θ. It is found from this figure that both the temperature and the thermal boundary layer thickness are the increasing function of λ. It is also noticed from Figures 10 and 11 that for large values of M and λ, the change in temperature is small, this is because both parameters have no influence on the energy equation, directly. The temperature field, $\theta(\eta)$, for several values of thermal slip parameter, γ, is shown in Figure 12. It is observed that as the thermal slip parameter increases, less heat is transformed from the sheet to the fluid, therefore the temperature $\theta(\eta)$ decreases by increasing the values of the thermal slip parameter, γ.

Table 2 shows the numerical values of the local Nusselt number $-\theta'(0)$ for various values of A and Pr when $M = \varepsilon = \lambda = \gamma = \beta = 0$, both numerically and analytically. In this table we have given a comparison with the existing numerical result of [13] and the relative error is also tabulated. One can easily see that the error is very much smaller which is almost negligible. Table 3 shows the numerical values of the skin-friction coefficient, $-f''(0)$, and the local Nusselt number $-\theta'(0)$ for various values of A, M and λ when $\varepsilon = 0.5$, $\gamma = \beta = 0.2$ and Pr = 0.5 both numerically and analytically. It is noted that the magnitudes of $-f''(0)$ and $-\theta'(0)$ are increased for large values of A.

It can also be seen from this table that the magnitudes of the shear stress at the wall, $-f''(0)$, increases by increasing the values of M and λ, but the rate of heat transfer at the wall decreases by increasing the values of both M and λ. The numerical values of $-f''(0)$ and $-\theta'(0)$ for several values of ε, β and A are given in Table 4. It is found that for fixed values of ε and β, both the magnitude of $-f''(0)$ and $-\theta'(0)$ are increased as the values of A increase. It is also seen that the magnitude of the skin-friction coefficient, $-f''(0)$, decreases for $\varepsilon < 1$ and it increases for $\varepsilon > 1$ for fixed values of A and β. On the other hand, the magnitude of $-f''(0)$ decreases as the velocity slip parameter, β, increases. However, the rate of heat transfer at the wall $-\theta'(0)$ is increased for large values of ε, where as it decreases by increasing the values of β. Table 5 is made to show the numerical values of the local Nusselt number $-\theta'(0)$ for different values of Pr, γ and A when $M = \lambda = \beta = 0.2$ and $\varepsilon = 0.5$. It is observed that for the fixed values of A, the magnitude of the local Nusselt number increases for large values of Pr and decreases as γ increases. It is also worth mentioning that the comparison of both solutions are given in these tables and found to be in good agreement.

4. Concluding remarks

In the present investigation, the heat transfer and MHD stagnation point flow of a viscous fluid over an unsteady stretching surface through a porous medium with flow/thermal slip conditions are studied. A similarity solution of the non-linear system of ordinary differential equations is obtained, both analytically using Homotopy Analysis Method (HAM), and numerically using shooting method. The effects of the various emerging parameters on the velocity and temperature distributions are shown through graphs. The values of skin friction coefficient and local Nusselt number are also given in tabular form. From this analysis, we have made the following observations:

- Both the velocity f' and the boundary layer thickness are decreased by increasing λ and M.
- The magnitude of the velocity f' decreases with an increase in slip parameter β.
- The temperature θ and the thermal boundary layer thickness decrease with an increase in Pr, while they increase with an increase in M and λ.
- The temperature θ decreases by increasing the values of thermal slip parameter, γ.

Acknowledgment

The authors are thankful to the anonymous reviewers for their useful comments to improve this paper.

References

1. Pal, D. "Combined effects of non-uniform heat source/sink and thermal radiation on heat transfer over an unsteady stretching permeable surface", *Commn. Nonlinear. Sci. Num. Sim*, **16**, pp. 1890-1904 (2011).
2. Sakiadis, B.C. "Boundary layer behavior on continuous solid surfaces: I. Boundary-layer equations for two-dimensional and axisymmetric flow", *AIChE. J.*, **7**, pp. 26-28 (1961).
3. Sakiadis, B.C. "Boundary layer behaviour on continuous solid surface: II. Boundary layer behavior on continuous flat surface", *AIChE. J.*, **7**, pp. 221-225 (1961).
4. Crane, L.J. "Flow past a stretching plane", *Z Angew Math Phy.*, **21**, pp. 645-647 (1970).
5. Tsou, F.K. and Sparrow, E.M. and Goldstein, R.J. "Flow and heat transfer in the boundary layer on a continuous moving surface", *Int J. Heat Mass Transfer.*, **10**, pp. 219-235 (1967).
6. Vleggaar, J. "Laminar boundary layer behavior on continuous, accelerating surface", *Chem Eng. Sci.*, **32**, pp. 1517-1525 (1977).
7. Gupta, P.S. and Gupta, A.S. "Heat and mass transfer on a stretching sheet with suction or blowing", *Canadian J. Chem Eng.*, **55**, pp. 744-746 (1977).
8. Soundalgekar, V.M. and Ramana, T.V. "Heat transfer past a continuous moving plate with variable temperature", *Warme-Und Stoffubertraguge.*, **14**, pp. 91-93 (1980).
9. Grubka, L.J. and Bobba, K.M. "Heat transfer characteristics of a continuous stretching surface with variable temperature", *J. Heat Transfer.*, **107**, pp. 248-250 (1985).
10. Ali, M.E. "Heat transfer characteristics of a continuous stretching surface", *Warme-Und Stoffubertraguge*, **29**, pp. 227-234 (1994).
11. Wang, C.Y. "Liquid film on unsteady stretching sheet", *Quart. J. Appl. Math.*, **48**, p. 601 (1990).
12. Elbashbeshy, E.M.A. and Bazid, M.A.A. "Heat transfer over an unsteady stretching surface", *Heat Mass Transfer*, **41**, pp. 1-4 (2004).
13. Sharidan, S., Mahmood, T. and Pop, I. "Similarity solutions for the unsteady boundary layer flow and heat transfer due to a stretching sheet", *Int. J. Appl. Mech. Eng.*, **11**, pp. 647-654 (2006).
14. Tsai, R., Huang, K.H. and Huang, J.S. "Flow and heat transfer over an unsteady stretching surface with non-uniform heat source", *Int. Com. Heat Mass Transfer*, **35**, pp. 1340-1343 (2008).
15. Aziz, Abd El "Radiation effect on the flow and heat transfer over an unsteady stretching sheet", *Int. Com. Heat Mass Transfer*, **36**, pp. 521-524 (2009).

16. Mukhopadhyay, S. "Effect of thermal radiation on unsteady mixed convection flow and heat transfer over a porous stretching surface in medium", *Int J. Heat Mass Transfer*, **52**, pp. 3261-3265 (2009).

17. Ishak, A., Nazar, R. and Pop, I. "Heat transfer over an unsteady stretching permeable surface with prescribed wall temperature", *Nonlinear Anal: Real World Appl.*, **10**, pp. 2909-2913 (2009).

18. Hayat, T., Qasim, M. and Abbas, Z. "Radiation and mass transfer effects on the magnetohydrodynamic unsteady flow induced by a stretching sheet", *ZNA.*, **65a**, pp. 231-239 (2010).

19. Ziabakhsh, Z., Domairry, G., Mozaffari, M. and Mahbobifar, M. "Analytical solution of heat transfer over an unsteady stretching permeable surface with prescribed wall temperature", *J. Taiwan Institute of Chemical Engineers*, **41**, pp. 169-177 (2010).

20. Mukhopadhyay, S. "Effect of slip on unsteady mixed convective flow and heat transfer past a porous stretching surface in medium", *Nuclear Engin. and Design.*, **241**, pp. 2660-2665 (2011).

21. Elabashbeshy, E.M.A. and Emam, T.G. "Effects of thermal radiations and heat transfer over an unsteady stretching surface embedded in a porous medium in the presence of heat source or sink", *Thermal Science*, **15**, pp. 477-485 (2011).

22. Sharma, R. "Effect of viscous dissipation and heat source on unsteady boundary layer flow and heat transfer past a stretching surface embedded in a porous medium using element free Galerkin method", *Appl. Maths. Comput.*, **219**, pp. 976-987 (2012).

23. Ibrahim, W. and Shankar, B. "Unsteady MHD boundary-layer flow and heat transfer due to stretching in the presence of heat source or sink", *Comp and Fluids*, **70**, pp. 21-28 (2012).

24. Khan, Y., Hussain, A. and Faraz, N. "Unsteady linear viscoelastic fluid model over stretching /shrinking sheet in the region of stagnation point flows", *Scientia Iranica*, **19**, pp. 1541-1549 (2012).

25. Reddy, G.V.R. and Reddy, N.B. "Mass transfer and MHD effects on unsteady porous stretching surface embedded in a porous medium with variable heat flux in the presence of heat source", *J. Appl. Comp. Sci. Math.*, **14**, pp. 49-54 (2013).

26. Liao, S.J., *Beyond Perturbation, Introduction to Homotopy Analysis Method*, Boca Raton: Chapman & Hall/CRC Press (2003).

27. Liao, S.J. "A uniformly valid analytical solution of 2D viscous flow past a semi-infinite flat plate", *J. Fluid Mech.*, **385**, p. 101 (1999).

28. Abbasbandy, S. and Zakaria, F.S. "Soliton solutions for the fifth-order KdV equation with the homotopy analysis method", *Nonlinear Dyn.*, **51**, p. 83 (2008).

29. Abbasbandy, S. and Parkes, E.J. "Solitary smooth solutions for the Camassa-Holm equation by means of homotopy analysis method", *Chaos, Solitons & Fractals*, **36**, p. 581 (2008).

30. Abbasbandy, S. "Homotopy analysis method for radiation equations", *Int. Com. Heat Mass Transfer*, **34**, p. 380 (2007).

31. Abbas, Z., Sheikh, M. and Sajid, M. "Mass transfer in two MHD viscoelastic fluids over a shrinking sheet in porous medium with chemical reaction species", *J. Porous Media*, **16**, pp. 619-636 (2013).

32. Abbas, Z., Wang, Y., Hayat, T. and Oberlack, M. "Mixed convection in the stagnation point flow of a Maxwell fluid towards a vertical stretching surface", *Nonlinear Analysis: Real World Appl.*, **11**, pp. 3218-3228 (2010).

33. Javed, T., Ahmed, I., Abbas, Z. and Hayat, T. "Rotating flow of a micropolar fluid induced by a stretching surface", *Zeitschrift fur Naturforschung A*, **65a**, pp. 829-836 (2010).

34. Abbas, Z. and Hayat, T. "Stagnation slip flow and heat transfer over a non linear stretching sheet", *Numer. Mech. for PDE's*, **27**, pp. 302-314 (2011).

35. Abbas, Z., Hayat, T., Sajid, M. and Asgher, S. "Unsteady flow of a second grade fluid film over an unsteady stretching sheet", *Mathematical and Computer Modelling*, **48**, pp. 518-526 (2008).

36. Abbas, Z., Wang, Y., Hayat, T. and Oberlack, M. "Hydromagnetic flow in a viscoelastic fluid due to the oscillatory stretching surface", *Int. J. Nonlinear Mechanic*, **43**, pp. 783-793 (2008).

37. Hayat, T., Abbas, Z. and Pop, I. "Momentum and heat transfer over a continuously moving surface with a parallel free stream in a viscoelastic fluid", *Numerical Methods for PDE's*, **26**, pp. 305-319 (2010).

38. Na, T.Y. *Computational Methods in Engineering Boundary Value Problems*, New York (1979).

Biographies

Zaheer Abbas is an assistant professor in Department of Mathematics, the Islamia University of Bahawalpur, Bahawalpur. He earned his PhD in applied mathematics from Quaid-I-Azam University, Islamabad, in 2010. His research interests include Newtonian and non-Newtonian fluids flow, fluid flow in porous medium, heat and mass transfer, magnetohydrodynamics and fluid dynamics of Peristaltic flows.

Noor Muhammad at present is Lecturer in Department of Mathematics, COMSATS Institute of Infor-

mation Technology, Attock. He attained his M.Phil in Applied Mathematics from International Islamic University, Islamabad, in 2011. His research interests includes the study of heat and mass transfer and fluid dynamics.

Ghulam Mustafa received a PhD (2004) in Mathematics from the University of Science and Technology of China, P.R. China. He also received his Post Doctorate from Durham University, UK, sponsored by Association of Commonwealth Universities, UK, 2011. Currently, he is Visiting Fellow of Chinese Academy of Sciences at University of Science and Technology of China. He is an Associate Professor in the Department of Mathematics, the Islamia University of Bahawalpur, Pakistan. His research interests include geometric modelling, applied approximation theory and solution of differential equations.